PARAMETRIC STUDY OF SOLAR AIR HEATER WITH DIFFERENT RIB GEOMETRIES

Thakur D.S., Khan M.K.* and Pathak M.
*Author for correspondence
Department of Mechanical Engineering,
Indian Institute of Technology Patna,
Bihta, 801103,
India
E-mail: mkkhan@iitp.ac.in

ABSTRACT

In the present work, A 2D CFD simulation using ANSYS FLUENT 15.0 have been performed to investigate the performance of flat plate solar air heaters with different rib geometries (artificial roughness) such as semi-circular, circular, rectangular and triangular (wedge) and hyperbolic rib with flat tip. In fact, the hyperbolic rib profile is the novelty in this work. The CFD model of smooth duct is validated with the Dittus-Boelter Nusselt number correlation and the Blasius equation for heat transfer and frictional pressure drop respectively. RNG k-ε model is used for turbulent modelling. The proposed hyperbolic rib profile gives best performance at low Re whereas rectangular profile is found to be best at high Re.

INTRODUCTION

In the present scenario, there is a need to exploit the renewable energy resources to meet the growing demand for energy to sustain the growth and development of nations. Solar energy is one such resource which could be tapped to fulfil this growing energy demand. Solar collectors have been used to convert solar energy into thermal energy since last few decades and efforts are being made to improve their performance. Numerous investigations have been performed worldwide to enhance thermo-hydraulic performance of solar air heaters [1-8]. Recently Suman et al. [9] published a comprehensive review of literature pertaining to solar collectors and their performance evaluation. In general, artificial roughness is created on the absorber plate to enhance surface area and turbulence near its surface which in turn enhances heat transfer rate. The ribs break laminar sublayer causing an intense mixing near the surface. As a result, there is an increase in heat transfer rate. However, in the process frictional pressure drop also gets increased.

On the basis of review, shape of rib, its height, pitch and their arrangement (inline or staggered) on the absorber plate do affect heat transfer and pressure drop characteristics significantly. With this in mind, a novel design of hyperbolic rib with flat tip has been evolved, which not only eliminates the entrapment of upstream eddies but also results in better thermo-hydraulic performance compared with rectangular, triangular and semicircular rib geometries.

NOMENCLATURE

c_p	[*J/kgK*]	Specific heat
H	[m]	Duct height
L	[m]	Length
W	[m]	Width of duct
p	[Pa]	Pressure
$\dot{q}''$	[W/m^2]	Heat flux
P	[m]	Pitch
T	[K]	Temperature
Q_u	[W]	Energy gain by air

Special characters

α	[deg]	Attack angle
ϕ	[deg]	Wedge angle
η	[-]	Thermo-hydraulic performance
μ	[N-s/m^2]	Viscosity of air

Subscripts

i	Inlet
o	Outlet
m	Arithmetic mean of inlet and outlet
f	roughened surface
s	Smooth surface
w	Absorber wall
0	Ambient or reference

MODEL DESCRIPTION

A 2D CFD analysis has been performed using ANSYS FLUENT on hyperbolic, rectangular, triangular and semicircular rib geometries, shown in Figure 1.

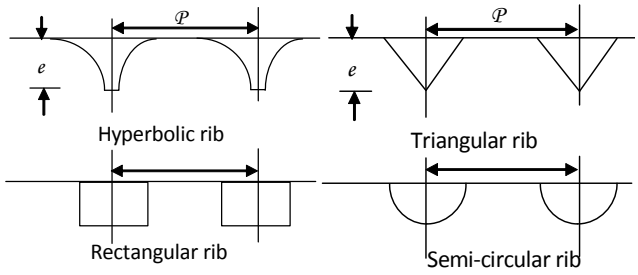

Figure 1 Rib geometries

The solar air heater geometry used in the present CFD simulation is shown in Figure2. It consists of absorber plate having length L_2, subjected to constant heat flux of 1000 W/m^2. The entrance length $L_1 = 5\sqrt{WH}$ and exit length $L_3 = 2.5\sqrt{WH}$ have been provided as per ASHRAE standard 93 [10]. The idea is to have fully developed flow all along the length of absorber plate and proper mixing of cold and hot air streams at its downstream.

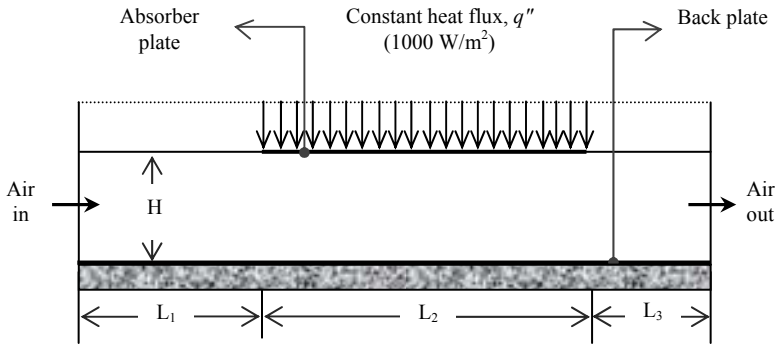

Figure 2 Schematic diagram of solar air heater

Following are the assumptions made:

- 2D, steady-state and fully developed turbulent flow
- Duct wall and rib material is aluminium, which is homogeneous and isotropic
- Thermal conductivity of absorber plate is constant
- Radiation and conduction heat losses are negligible

Values of geometrical used in the present simulation are shown in Table 1.

Table 1 Geometrical parameters

Parameter	*Value (mm)*
Entrance length of duct	225
Absorber plate length	275
Exit length of duct	121
Width of duct	100
Depth of duct	20
Hydraulic diameter	33.33

Governing Equations

Mass conservation or continuity equation

$$\frac{\partial}{\partial x_j}\left(u_j\right) = 0 \tag{1}$$

Momentum conservation or Navier-Stokes equation

$$\frac{\partial\left(\rho u_i u_j\right)}{\partial x_j} = -\frac{\partial p}{\partial x_i} + \mu\frac{\partial}{\partial x_j}\left(\frac{\partial u_i}{\partial x_j} + \frac{\partial u_j}{\partial x_i}\right) + \frac{\partial\left(-\rho\overline{u_i' u_j'}\right)}{\partial x_j} \tag{2}$$

Energy conservation equation

$$\frac{\partial\left(u_j T\right)}{\partial x_j} = \alpha\frac{\partial}{\partial x_j}\left(\frac{\partial T}{\partial x_j}\right) + \frac{\mu_t}{\rho\sigma_t}\frac{\partial}{\partial x_j}\left(\frac{\partial T}{\partial x_j}\right) \tag{3}$$

The boundary conditions employed in the code are shown in Table 2.

Table 2 Boundary conditions

Location	**Boundary condition**	**Value**
Inlet	Velocity (u)	1.72- 7.88 m/s
	Temperature	300 K
Absorber plate	Velocities	$u = v = 0$ m/s
	Heat flux	1000 W/m^2
Other walls (all insulated)	Velocities	$u = v = 0$ m/s
	Heat flux	0 W/m^2
Outlet	Pressure	p_{atm}

Numerical Methodology

Simulations have been performed using finite volume based commercial CFD software ANSYS FLUENT 15.0. Steady pressure based solver has been used to solve the governing equations in a sequential manner. The momentum and energy equations have been discretized with second order upwind scheme. For pressure-velocity coupling SIMPLE (Semi Implicit Pressure Linked Equation) algorithm has been used. For turbulent modelling, RNG k-ε model with enhanced wall treatment has been employed. Sum of residual mass and residual energy must be less than $10^{-6}$and 10^{-9} respectively for the convergence of solution.

Grid independence test has been conducted by varying mesh size from 13781 to 313245. The results have been found to be independent of grid at 220147. However, to capture the laminar sublayer near wall a finer mesh of size 313245. For the meshing we have used structured non-uniform mesh with quadrilateral element.

RESULTS AND DISCUSSION

This section has been divided into three sections, viz. model validation, parametric study and flow visualization.

Model Validation

The proposed CFD model is validated with the following well-established smooth duct correlations:

Dittus-Boelter Nusselt number correlation [11] for heat transfer:

$$Nu = 0.023\,\mathrm{Re}^{0.8}\,\mathrm{Pr}^{0.4} \tag{4}$$

Blasius friction factor correlation [11] for frictional pressure drop:

$$f = 0.316\,\mathrm{Re}^{-0.25} \tag{5}$$

Heat transfer and pressure drop characteristics are obtained by evaluating Nusselt number and friction factor for the flow inside the duct.

Using the temperature data obtained from CFD simulation, the average heat transfer coefficient h is computed by applying energy balance:

$$Q_u = \dot{m}c_p\left(T_o - T_i\right) = hA\left(T_w - T_m\right) \tag{6}$$

The average Nusselt number is given by

$$Nu = \frac{hD_h}{k} \tag{7}$$

In order to evaluate friction pressure data (inlet and outlet of duct) from the CFD model is extracted and Darcy-Weisbach equation is used to evaluate Darcy friction factor *f*, i.e.

$$\Delta p_f = f \frac{L}{D_h}\left(\frac{1}{2}\rho V^2\right) \tag{8}$$

where, V is average fluid velocity inside the duct

Δp_f is difference between inlet and outlet fluid pressure

The computed values of friction factor and Nusselt number have been compared with the corresponding values obtained from Blasius and Dittus-Boelter correlations in Figure 3. The percentage mean deviations in friction factor and Nusselt number are 1.59 and 2.94 respectively. With deviations being small, it can be concluded that the proposed numerical model is in good agreement with the well-established correlations for friction factor and Nusselt number.

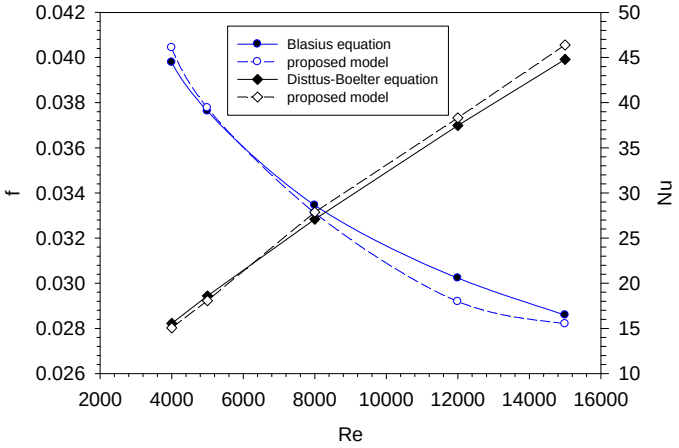

Figure 3 Validation of model

Parametric Study

As a matter of fact that provision of ribs increases both heat transfer and frictional pressure drop. Higher heat transfer is desirable whereas higher pressure drop entails higher pumping power. Thus, Webb and Eckert [1] defined a parameter known as thermo-hydraulic performance parameter η which relates heat transfer rate with pressure drop in the following manner:

$$\eta = \frac{Nu_f / Nu_s}{\left(f_f / f_s\right)^{1/3}} \tag{9}$$

It relates combined effect of heat transfer and pressure drop in a frictional duct with that in a smooth duct. Higher the value of thermo-hydraulic performance parameter better is the performance.

The parameters such as rib height and pitch for novel hyperbolic rib geometry with flat tip have been varied to optimize the heat transfer and pressure drop characteristics. For rib height e = 1 mm and pitch P = 10 mm, the thermo-hydraulic performance is found to be the best. Figure 4 shows the comparison of performance of novel hyperbolic rib geometry with rectangular, triangular and semicircular rib geometries for e = 1 mm and P = 10 mm. The performance is presented in terms friction factor, heat transfer coefficient and thermohydraulic performance parameters. A comparison is also with smooth duct.

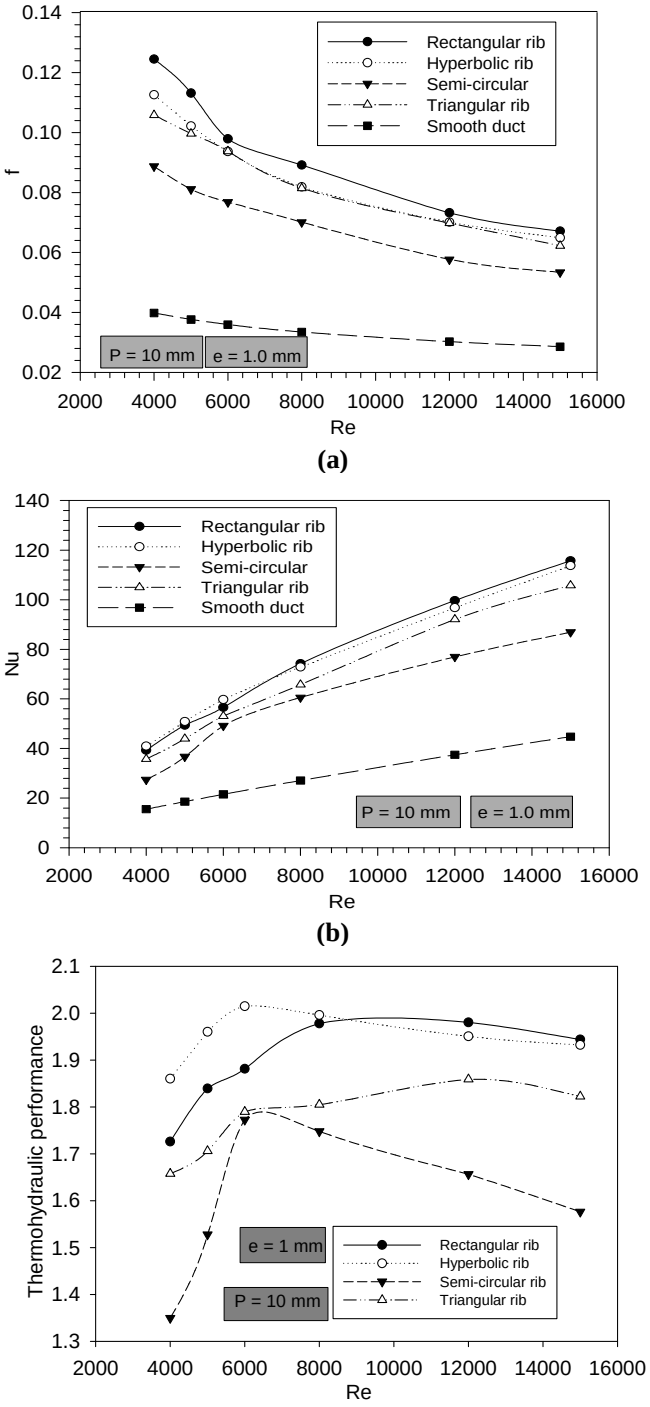

Figure 4 Performance comparison (a) f versus Re (b) Nu versus Re (c) ηversus Re.

Figure 4(a) shows the variation of friction factor f with Re for different rib geometries. For any rib shape, friction factor decreases with the increase in Re. In fact, the rectangular rib has the highest value of friction factor for any Re followed by hyperbolic, triangular and semicircular ribs. Semi-circular ribs have the best performance as far as frictional pressure drop is concerned. Figure 4(b) shows the variation of heat transfer coefficient or Nu with Re for different rib geometries. The hyperbolic rib geometry has the highest heat transfer coefficient at low Re flows. However, heat transfer coefficient is highest for rectangular geometry at high Re flow. Heat transfer characteristics of other geometries are inferior with semicircular rib has the least heat transfer coefficient. Thus the performance of semicircular rib as far as heat transfer is concerned is the worst. To have the true picture of performance, thermohydraulic parameter for each geometry has been evaluated and plotted in Figure 4(c). The thermo-hydraulic performance is best for hyperbolic rib geometry at low Re whereas it is best for rectangular rib at high Re. Thermohydraulic performance is found to be worst for semicircular rib geometry for any Re.

To understand the physics behind such behaviour, the flow patterns for each rib geometry have been investigated and shown in Figures 5 and 6.

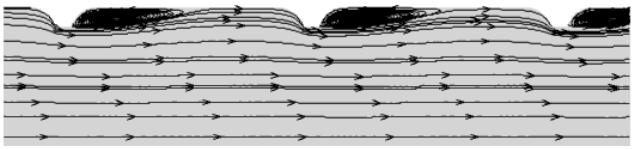

Re 4000

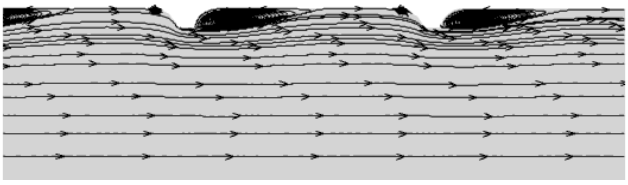

Re 6000

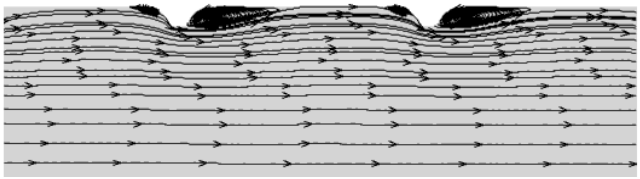

Re 15000

Figure 5 Streamline contours for different Re at P = 10 mm and e = 1mm

Streamline contour plots have been drawn in Figure 5 to show the effect of Re on the recirculation zones near each rib. A big recirculation zone appears at the downstream of each rib due to the separation of boundary layer leading to the formation of eddies (recirculation zone). The separation causes an increase pressure drop whereas eddies flow or recirculation causes an increase in heat transfer rate as it causes mixing. The pitch should be large enough to avoid entrapment of eddies between the adjacent ribs. Local heat transfer coefficient varies along the surface of absorber plate. Local heat transfer coefficient as well as local skin friction coefficient is maximum at the point of reattachment of boundary layer between the ribs whereas they decrease as the boundary layer develops in the direction of flow. It can be seen clearly from Fig. 5 that recirculation zone decreases with the increase in Re due to which pressure drop across each rib decreases resulting in an overall drop in pressure across the duct, which is evident from reducing friction factor with Re (Figure 4(a)). Further a small recirculation zone starts appearing in the upstream of rib with increase in Re. This would result in further increase heat transfer rate.

A comparison of flow patterns at Re = 6000 for hyperbolic, rectangular and triangular ribs is shown in Figure 6. The semicircular ribs have not been shown here. Sizes of recirculation zones in hyperbolic and rectangular ribs are comparable whereas that of triangular is larger and that may be the reason why the pressure drop effects become more dominant than heat transfer effects resulting in its poor thermohydraulic performance

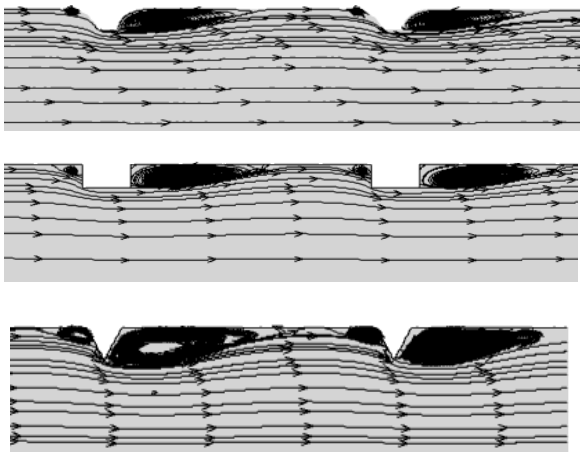

Figure 6 Streamline contours for different rib geometry

The isothermal contours for hyperbolic, rectangular and triangular rib geometries have been shown in Figure 7 for Re = 6000, e = 1 mm and P = 10 mm. Temperature distribution is near the surface tells the local variation in heat transfer coefficient. Lower local plate surface temperature is the proof of higher local heat transfer or vice versa. Hotspots (red in colour) can be seen in the root of rib profile. It may be due to the entrapment of eddies in the corners. Since heat flux is const at the surface, the local variation in surface temperature is attributed to the local variation in heat transfer coefficient, which is dependent upon the flow patterns formed near the surface. Each rib geometry has recirculation zones of different sizes and shapes. Accordingly the pressure drop varies from rib to rib.

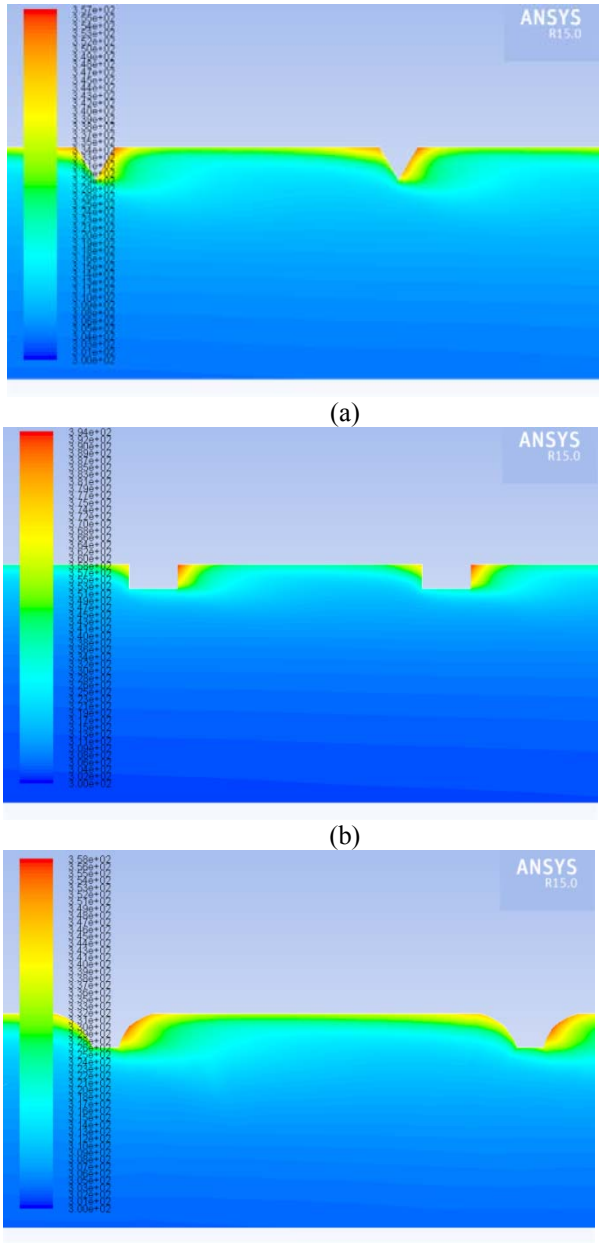

Figure 7 temperature contours for different rib (a) triangular rib, (b) rectangular rib and (c) hyperbolic rib.

Figure 8 and 9 show the variations of surface velocity gradient (a measure of local wall shear stress or frictional pressure drop) and local heat transfer coefficient along the absorber plate length for hyperbolic rib profile with Re = 6000, e = 1 mm and P = 10 mm.

The velocity gradient at the wall helps in identifying whether the flow is attached or detached. The flow over the rib accelerates till its peak and should decelerate beyond that. However, due to existence of adverse pressure gradient in the downstream, boundary layer could not follow the rib contour and flow separation takes place. The separation is marked by local recirculation of flow in the form of eddies. The flow reattaches itself after a certain distance from the rib. Peaks and valleys show the separation and reattachment of flow across different ribs.

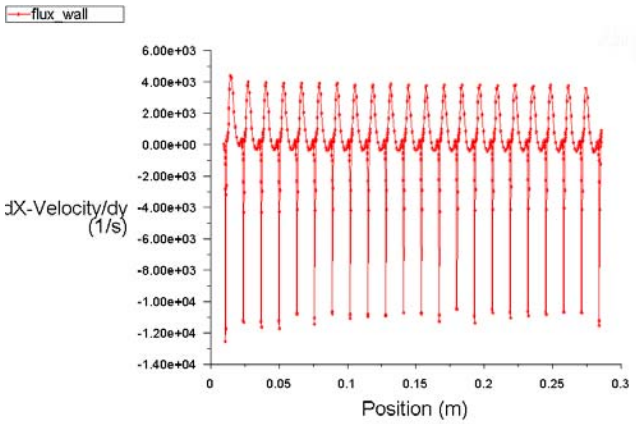

Figure 8 Variation of surface velocity gradient along the absorber plate length

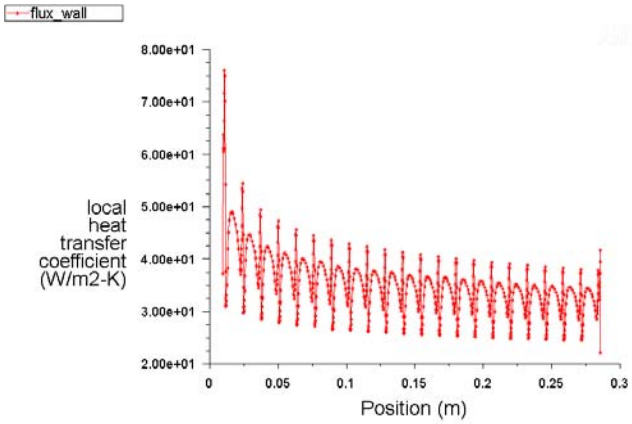

Figure 9 Variation of local heat transfer coefficient along the absorber plate length

Figure 9 shows the corresponding variation in local heat transfer coefficient along the absorber plate. Heat transfer coefficient strongly depends upon the variations in local velocity near the absorber plate surface. The local heat transfer coefficient is maximum at the point of reattachment in the inter-rib spacing already mentioned before.

CONCLUSION

In this paper, a numerical investigation of novel hyperbolic rib profile with flat tip has been carried out using ANSYS FLUENT 15.0. For optimized rib height and pitch (i.e. e = 1mm and P = 10 mm), the comparison of the performance of this novel rib profile has been done with rectangular, triangular and semicircular rib profiles in terms of friction factor, heat transfer coefficient and thermohydraulic performance parameter. The proposed hyperbolic rib profile gives best performance at low Re whereas rectangular profile is found to be best at high Re.

REFERENCES

[1]R.L. Webb, E.R.G. Eckert, Application of rough surface to heat exchanger design, *International Journal of Heat and Mass Transfer*, 15 (9) (1972), pp. 1647–1658

[2] B.N. Prasad, J.S. Saini, Effect of artificial roughness on heat transfer and friction factor in a solar air heater, Solar Energy, 41 (1988), pp. 555–560

[3]V.S. Hans, R.P. Saini, J.S. Saini, Performance of artificially roughened solar air heaters—A review, Renewableand Sustainable Energy reviews,13(2009), pp 1854–1869

[4] B.N. Prasad, J.S. Saini, Optimal thermo-hydraulic performance of artificial roughened solar air heater, Solar Energy, 47 (2) (1991), pp. 91–96

[5] K. Yakut, N. Alemdaroglu, B. Sahin, C. Celik, Optimum design-parameters of a heat exchanger having hexagonal fins, Applied Energy, 83 (2006), pp. 82–98

[6] S. Yadav, J.L. Bhagoria. A CFD based thermo-hydraulic performance analysis of an artificially roughened solar air heater having equilateral triangular sectioned rib roughness on the absorber plate, *International Journal of Heat and Mass Transfer*,70(2014), pp.1016-1029

[7] Almogbel M., and Bejan A., Cylindrical trees of pin fins, *International Journal of Heat and Mass Transfer*, Vol. 43, 2000, pp. 4285-4297

[8] M.K. Mittal, Varun, R.P. Saini, S.K. Singhal, Effective efficiency of solar air heaters having different types of roughness elements on the absorber plate, Energy, 32 (2007), pp. 739–745

[9] American Society of Heating, Refrigerating and Air Conditioning Engineers. ASHRAE Standard 93 GA30329 Method of testing to determine the thermal performance of solar collectors. Atlanta: ASHRAE, 2003

[10]W.H. McAdams, Heat Transmission, McGraw-Hill, New York (1942)

[11] S.Suman, M. K. Khan, M. Pathak, Performance enhancement of solar collectors—A review, Renewableand Sustainable Energy reviews,49(2015), pp 192-210

[12] ANSYS 12.0 User's Guide, ANSYS Inc. April 2009